Mitigation of Spatial Effects on an Area-Based Lidar Forest Inventory (2024)

Jacob L. Strunk, Diogo N. Cosenza, Francisco Mauro, Hans-Erik Andersen, Sytze de Bruin, Timothy Bryant, and Petteri Packalen

***Abstract*—Different sizes and shapes of field plots relative to raster grid cells were found to negatively affect lidar augmented forest inventory. This issue is called the "change of spatial support problem (COSP)" and caused biases and reduction in estimation efficiency (precision per number of plots). For a ∼14 000 km^2 study area in Oregon State, USA, we examined three different plot shapes, both fixed-radius and cluster plots, alongside grid cell sizes ranging from 5 to 70 m. Effect size varied with the magnitude of spatial mismatch between plots and raster grid cells. There was up to 15% bias and a 98% reduction in estimation efficiency. Fortunately, no negative effects were observed for circle (plots) versus square (grid cell) shaped regions with the same areas (m^2). This study contributes to the sparse body of literature around change of spatial support in the area-based approach to lidar forest inventory and provides methods to easily avoid and mitigate negative effects. The simplest approach to avoid bias, although not always practical or feasible, is to exactly match the area (m^2) of circular field plots and raster grid cells. Use of metrics robust to spatial effects, such as median height and height ratios, can also reduce change of spatial support effects. Finally, we demonstrate that attribution of plots directly from raster grid cells (the "raster-intersect" approach) is robust to change of spatial support and flexible in application, but sacrifices a small amount of predictive power (a glossary of technical terminology is also provided in the appendix).**

***Index Terms*—Airborne laser scanning (ALS), area-based approach (ABA), change of spatial support problem (COSP), estimation, lidar forest inventory, model-assisted, modifiable areal unit problem (MAUP).**

I. Introduction

AIRBORNE lidar scanning (henceforth referred to as "lidar") is an active remote sensing technology based around a lidar sensor (a glossary of technical terminology is also provided in the appendix). The lidar sensor, mounted to an airborne platform, typically a fixed-wing aircraft, is used to scan the environment including vegetation. The lidar scans yield dense three-dimensional measurements (point clouds) of the ground and vegetation. Lidar data can then be used as auxiliary information to support various forest inventory applications [1]. This study is focused on the area-based approach (ABA), which is arguably the most common way to augment forest inventory. ABA lidar forest inventory has been implemented around world, e.g., [2], [3], [4]. In ABA lidar forest inventory, inferences about the forested landscape are based on "areas," especially fixed radius field plots and grid cells (grid cells are square tessellations of the project area stored as pixels in geospatial rasters). ABA is distinct from individual tree detection (ITD) approaches in which lidar is used to infer properties of individual trees, e.g., [5], [6], [7]. Hybrid ABA-ITD strategies are also feasible, e.g., [8]. The ABA approach to forest inventory with lidar is also widely used by public organizations in the Pacific Northwest region of the USA.

ABA lidar forest inventory requires paired field-based and remote-sensing-based measurements for forest inventory plots. The paired measurements are used to link forest attributes to lidar point cloud-based statistics (or "lidar metrics") such as height statistics and ratios. Models linking the two types of measurements (field based and remote sensing-based) are then used to help in estimation of forest attributes, such as volume, biomass, carbon, tree heights, and trees per hectare. In the final step in ABA, fitted models are used for predictions to lidar metrics computed for grid cells for the entire study area. In an ideal world, the sizes and shapes of the grid cells and field plots would be identical, but as pointed out by Packalen et al. [9], this is not always the case. There are often size and shape mismatches between field plots and raster grid cells, which may negatively affect accuracy and precision.

The mismatch in the sizes and shapes of field plots and raster grid cells falls into an active area of research around the "change of support problem" or "change of *spatial* support problem (COSP)" [10], [11], [12], [13]. However, the effects of change in spatial support on ABA lidar forest inventory are only sparsely addressed in the research literature.

The general idea behind the widely studied COSP is that the size and shape of the measurement region (e.g., forest inventory plots and raster grid cells) may affect the expected attribute values. As a result, inferences for measurements collected with

Received 12 February 2024; revised 19 November 2024; accepted 7 January 2025. Date of publication 16 January 2025; date of current version 14 February 2025. This work was supported by the USDA Forest Service. *(Corresponding author: Jacob L. Strunk.)*

Jacob L. Strunk is with the USDA Forest Service Pacific Northwest Research Station, Olympia, WA 98512 USA (e-mail: jacob.strunk@usda.gov).

Diogo N. Cosenza is with the Department of Forest Engineering, Federal University of Viçosa, Viçosa 36570-900, Brazil (e-mail: diogo.cosenza@ufv.br).

Francisco Mauro is with the iuFOR, EiFAB, Campus de Soria, Universidad de Valladolid, 42004 Soria, Spain (e-mail: francisco.mauro@uva.es).

Hans-Erik Andersen is with the USDA Forest Service Pacific Northwest Research Station, University of Washington, Seattle, WA 98195-2100 USA (e-mail: hans.andersen@usda.gov).

Sytze de Bruin is with the Laboratory of Geo-Information Science and Remote Sensing, Wageningen University, 6708 PB Wageningen, Netherlands (e-mail: sytze.debruin@wur.nl).

Timothy Bryant is with the USDA Forest Service Pacific Northwest Region, Portland, OR 97204 USA (e-mail: timothy.bryant@usda.gov).

Petteri Packalen is with the Bioeconomy and Environment Unit, Natural Resources Institute Finland (Luke), FI-00790 Helsinki, Finland (e-mail: petteri.packalen@luke.fi).

Digital Object Identifier 10.1109/JSTARS.2025.3528834

different sizes and shapes may be biased. In spatial statistics, the "support" or "spatial support" of measurements is characterized by the size, shape, and orientation (orientation is not addressed) of the measurements [14, p. 640]. For example, different spatial supports for lidar metrics could include a 30 × 30 m grid of square cells, a 5 × 5 m grid of hexagonal grid cells, or a 10 km grid of cluster plots. The change in spatial support *problem* then is when a change in the size or shape of the measurement area results in a practically significant change in the values of a measured attribute [11], [12], [15]. For example, the maximum tree height on plots is expected to be taller on average for a larger plot (e.g., 0.1 ha) than for a smaller plot (e.g., 0.01 ha) plot. The COSP is highly relevant to ABA lidar forest inventory because it is commonplace to measure trees on a plot size that is different from the raster grid cell size used for prediction and estimation.

In the typical lidar ABA workflow, plots are attributed from lidar points clipped to match the plot shape, which is typically circular. We will henceforth refer to this as the "point-clip" approach in which lidar metrics, such as height quantiles and cover ratios, are computed for lidar points from the exact plot footprints. The lidar metrics computed for area-wide predictions, in contrast, are typically for square grid cells that are stored in raster layers. Fortunately, Packelen et al. [16] found that so long as circular plots and square grid cells had the same areas, there was no practical difference between the lidar metrics on average.

Mauro et al. [17] proposed a simplified alternative to the point-clip workflow that may alleviate COSPs due to different plot and grid cell shapes and sizes. They proposed to attribute plots directly from raster grid cells of lidar metrics that intersect the plot. We will henceforth refer to this as the "raster-intersect" approach. The raster-intersect approach workflow with lidar resembles the typical workflow used in image-based remote sensing analyses. In the rasters-intersect approach, there is a better spatial correspondence between modeling and prediction datasets, since the same raster grid cells are used for both cases. The raster-intersect approach is also simpler than the point-clip approach since there is no need to clip out lidar points for plot locations and compute their lidar metrics.

An important step in both point-clip and raster-intersect approaches to ABA forest inventory is the accurate positioning of field plots. Otherwise, field and remote sensing measurements may not correspond to the same patch of forest. To maximize the correspondence between field and remote sensing measurements (i.e., spatial coregistration) and thus the potential of the models, field plots should be carefully surveyed with high-performance GNSS (HPGNSS; [18]). HPGNSS involves the combination of equipment and protocols required to achieve better than 1 m accuracy in the forest.

While it has been demonstrated that ABA models built using the traditional point-clip workflow can be affected by plot size [15], [19] and positioning accuracy [19], [20], the effects of a raster-intersect workflow on ABA inferences are not well known and should be investigated as a possible alternative.

The modifiable areal unit problem (MAUP) is another actively researched topic and is closely related to the change of support problem [21], [22], [23]. The MAUP deals with the effect of measurement scale and aggregation unit (e.g., fine to coarse) on the resulting inferences about relationships among variables. An example of the MAUP in the context of this study would be an effect of plot size on model coefficients that relate forest biomass to lidar metrics. Researchers have studied the MAUP in the context of model fit performance for ABA lidar inventories (although they do not explicitly mention it), but with conflicting results. Ozkan and Demirel [24] and Packalen et.al. [9] observed minimal effect from plot size on model fitting, while Frazer et al. [19] and Mauya et al. [15] concluded that larger plot sizes performed better. The disparity in findings may be related to their different vegetation conditions or different plot location accuracies.

ABA methods are widely used in lidar forest inventory, but there is little guidance in the body of related research publications on the magnitude of effects from changes of spatial support, especially plot versus grid cell sizes and shapes. However, understanding the COSP methods in ABA lidar forest inventory is critical to decisions about sample plot size and shape, and use of appropriate analytical methods. This study sheds new light on the COSP for ABA lidar forest inventory. We quantify the effects of changes in spatial support and plot attribution methods (point-clip versus raster-intersect) on components of ABA lidar forest inventory, including

1) distributions of lidar metrics,
2) variable selection and model fitting, and
3) estimation performance.

Our analysis is performed for the forest attributes basal area (BA, m^2/ha), bole volume (VOL, m^3/ha), carbon (C, Mg/ha), quadratic mean diameter (QMD, cm), stand density index (SDI, $\mathrm{trees}/\mathrm{ha}$), and number of trees per ha (TPH, $\mathrm{trees}/\mathrm{ha}$). This study uses both precisely georeferenced national forest inventory plot data for the United States and a separate USFS forest inventory modeling dataset with large 0.1 ha plots designed specifically for use with lidar. Our inferences provide practitioners with the practical implications of changes in spatial support (plots versus raster grid cells), as well as guidance on how to avoid or mitigate negative consequences from changes in spatial support.

II. Methods

A. Study Site

The ∼14 000 square kilometer study area is located primarily in temperate mixed conifer forests on the western slope of the Cascade Mountains in Oregon State, USA (see Fig. 1). Dominant tree species include Douglas-fir (*Pseudotsuga menziesii*), ponderosa pine (*Pinus ponderosa*), white fir (*Abies concolor*), and pacific silver fir (*Abies amabilis*).

B. Field Data

This study uses two distinct sets of forest inventory plots with different plot configurations and grid layouts that enable us to assess plot size and shape effects. The first is a set of 1011 m^2 circle forest inventory plots installed by the U.S. Forest Service specifically to model forest structure from lidar data, henceforth referred to as "large plots" (Fig. 2, leftmost pane). A total of 288 large plots were measured in the study area from 2016–2018, with the greatest proportion measured in 2016. The second set of 264 forest inventory plots comes from the Forest Inventory Analysis (FIA) national forest inventory [25], which uses cluster

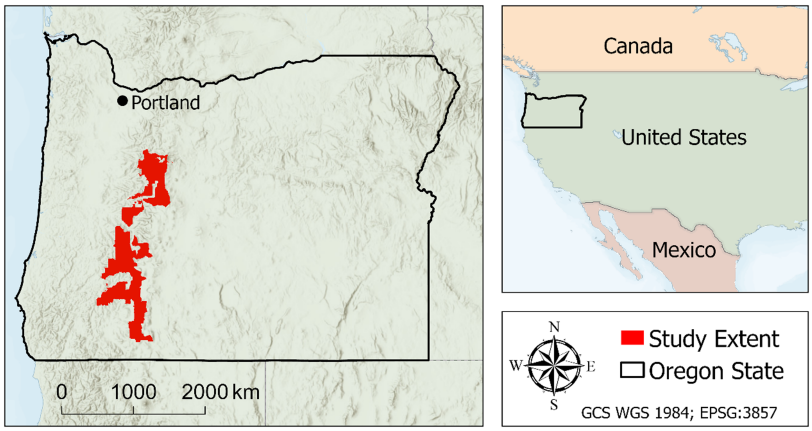

Fig. 1. Project extent in southwestern Oregon State in the USA.

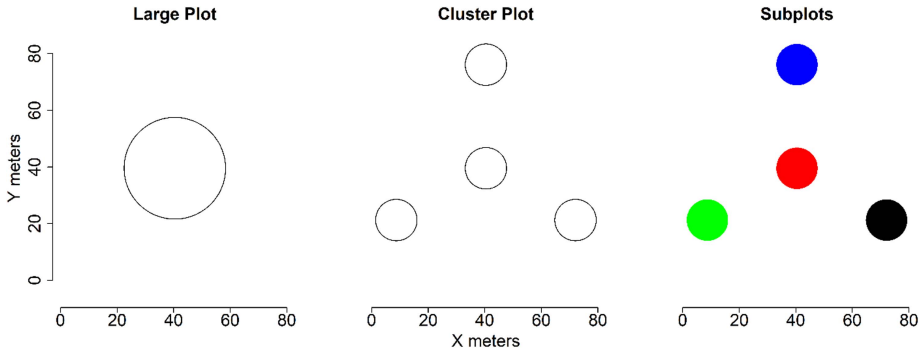

Fig. 2. Field plot configurations used for analyses where the smallest "plot" size is actually subplots from the cluster plot.

TABLE I
DESCRIPTIVE STATISTICS INCLUDING MEANS AND STANDARD DEVIATIONS (IN PARENTHESES) BY PLOT TYPE FOR ALL OF THE RESPONSE VARIABLES EXPLORED

		Mean (SD) by plot type		
Response	Units	Large	Cluster	Subplot
Basal area	m^3 ha^{-1}	46.0 (22.7)	45.8 (27.5)	46.8 (31.0)
Carbon	Mg ha^{-1}	189.4 (109.4)	184.1 (133)	188.3 (144.8)
Quadratic mean diameter	cm	43.8 (15.5)	46.0 (18.0)	45.4 (23.5)
Stand density index	trees ha^{-1}	875.4 (423.4)	915.3 (464.9)	876.7 (531.3)
Trees per hectare	trees ha^{-1}	367.3 (215.8)	383.1 (218.1)	389.8 (285.4)
Bole volume	m^3 ha^{-1}	546.7 (335.2)	540.8 (394.1)	553.1 (441.3)

Large, cluster, and subplot types had 288, 264, and 1011 observations respectively.

plots consisting of 4 × 168 m^2 subplots with a total area of 674 m^2, henceforth referred to as "cluster plots" (Fig. 2, center pane). Some analyses also involved individual subplot-level attributes, which are henceforth referred to as "subplots." Three years of cluster plots and subplots (2015–2017) were used. Forest attributes were derived from field measurements for each plot design using the Forest Vegetation Simulator [26]. Descriptive statistics for forest attributes by plot type are provided in Table I.

All plot locations were recorded using procedures and equipment consistent with FIA's definition of high performance GNSS positioning in the forest (e.g., use of tripods, 20+ minute occupations, 1-second recording rate, survey grade GNSS receivers, differential post-processing), as described in detail by Andersen et al. [18].

C. Lidar Metric Computation

Metrics were obtained using the "stdmetrics_rn" and "stdshapemetrics" functions from the lidR package [27] and the "experimental_metrics" function in the RSForTools package

TABLE II
REPRESENTATIVE LIST OF LIDAR METRIC NAME ABBREVIATIONS AND DEFINITIONS

Lidar metrics	Descriptions
htmn, htmin, htmax, htsd, … **xmn, xmin, xmax, ysd, …** **ymn, ymin, ymax, ysd, …**	simple statistics for heights and x,y coordinates including, e.g., mean (mn), min, max, sd, and others
htP1, htP5, …, htP95 , htP99	lidar height quantiles
cover1	lidar cover, the ratio of returns above 1m to all returns
htRat1, htRat2, …, htRat50	ratios of height counts above 2, …, 50 m to all points above 1m
htRat1_2, htRat2_4, htRat4_5, …, htRat50+	ratios of point counts in bands to all 1-2, …, 50+ to all point
xymn, xymin, xysd, …	various simple statistics on the products of x and y including mean (mn), min, max, sd
xyzmn, xyzmin, xyzsd, …	various simple statistics on the products of x, y, and z including mean (mn), min, max, sd
xymnRt, xyminRt, xysdRt, …	square root transformation of simple statistics on x, y coordinates
grdArea, grdVol, voxVol, srfCover, srfArea, …	area, volume, and cover related statistics computed using 5m grid cells (grd), voxels (voc), and surfaces (srf)
xyAreaScl, voxVolScl, gridVolScl, areaCvrScl, srfAreaScl, …	area and volume statistics scaled by (divided by) their respective areas or volumes respectively
p1st, p2nd, p3rd, p4th, p5th	return count proportions by return number
eig1, eig2, eig3	first, second, and third eigen vectors computed on raw x, y, z values
curv, lnrty, plnrty, sphrcty, anstrpy, hzntlty	curvature, linearity, planarity, sphericity, anisotropy, horizontality; mathematical properties of point clouds derived from eigenvectors 1-3

Metrics other than "cover" metrics use only points with heights greater than 1m.

[28] for the *R* statistical programming language [29]. A total of 98 lidar metrics (see Table II) for this analysis were compiled to support exploratory analyses of lidar metrics for use in ABA lidar forest inventory. We expect that many of the supplied metrics are not suited for use as explanatory variables, but we erred on the side of casting a wide net in our exploration of lidar metrics.

D. Remote Sensing Plot Attribution

Lidar metrics were computed for various plot and grid cell sizes and shapes in support of our analyses. These shapes and sizes serve three purposes, including to provide population distributions of lidar metrics, to attribute field plots for forest modeling, and to assess prediction distributions, often interacted with by users in the form of a map. Plot attribution was conducted in two ways: by clipping the exact plot footprint corresponding to a plot location on the ground ("point-clip"), and by intersection of raster cells to the plot location ("raster-intersect") (see Fig. 3). In the case of raster-intersection with the plot, a weighted average was computed from intersecting cells based on their proportion of intersection with the plot footprint. Summaries of the plot shapes and sizes evaluated are provided in Table III.

E. Virtual Plot Design

To explore the effects of plot shapes and sizes on lidar metrics, approximately 10 000 virtual plots were distributed across the study area on a regular grid. At each virtual plot location, lidar metrics were computed using point-clip and raster-intersect approaches for various sizes of circle and square plots, as well as for cluster plots with both circle and square subplots (see Fig. 4). The two cluster plot designs have the nominal areas and layouts of United States Forest Service, Forest Inventory Analysis (USFS FIA) plots, except one of the designs uses square subplots instead of circular. The dimensions of the various plots shapes and sizes are provided in Table III.

F. Change of Support Effect on Lidar Metrics

The effects of changes in spatial support on lidar metrics are diagnosed both visually and numerically. In the visual diagnostic, e.g., Fig. 5, the mean value of the metric for 10 000 virtual plots is shown for different plot and pixels areas on the *X*-axis. A change in the average value of a lidar metric for a different plot size indicates a change of spatial support effect, e.g., the blue line in Fig. 5. No change in lidar metrics as a function of plot or grid cell areas indicates a spatial support effect and no trends indicate robustness to change of spatial support effects, e.g., the red line in Fig. 5 does not change with plot or grid cell area.

While visual diagnostics are highly informative, they are not conducive to evaluation of tens to hundreds of auxiliary variables and are difficult to rank objectively. To facilitate comparisons of sensitivity to changes in spatial support quickly and objectively for many lidar metrics, we also report the coefficients of variation

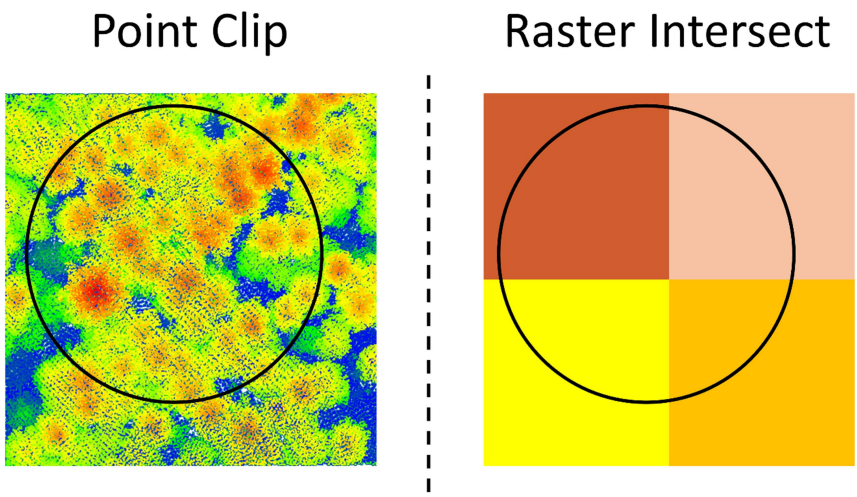

Fig. 3. Plot attribution by clipping lidar points within the plot bounds ("Point Clip" approach) and by intersection with a lidar-derived raster layer ("Raster-intersect" approach). In the point clip approach, statistics (lidar metrics) are computed from the lidar points falling within the plot boundary. In the raster-intersect approach, lidar metrics are computed from lidar points within each raster cell, and then a simple or area-weighted average is assigned to the plot.

TABLE III
PLOT AND GRID CELL DIMENSIONS

square side		circle radius		area	
meters	feet	meters	feet	ha	ac
70.0	229.7	39.5	129.6	0.490	1.211
60.0	196.9	33.9	111.1	0.360	0.890
50.0	164.0	28.2	92.6	0.250	0.618
40.0	131.2	22.6	74.0	0.160	0.395
31.8	104.4	17.9*	58.9	0.101	0.250
30.0	98.4	16.9	55.5	0.090	0.222
26.0	85.2	14.7*	48.1	0.067	0.167
20.0	65.6	11.3	37.0	0.040	0.099
13.0	42.7	7.3*	24.1	0.017	0.042
10.0	32.8	5.6	18.5	0.010	0.025
5.0	16.4	2.8	9.3	0.003	0.006
4x13	4x42.7	4x7.3*	4x24.1	0.068	0.167

*corresponds to field-measured plot dimensions.

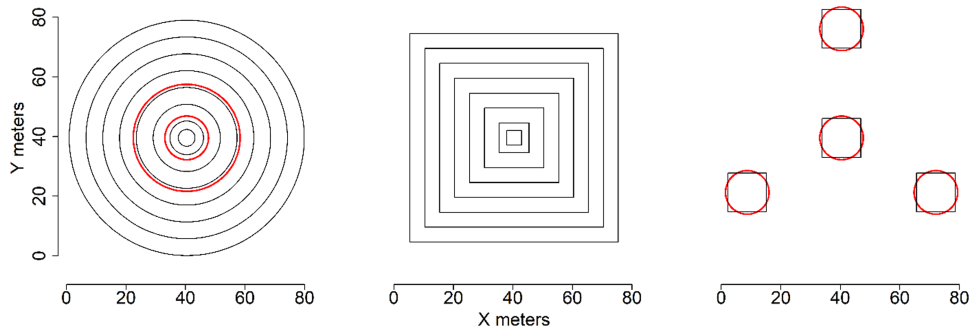

Fig. 4. Remote sensing plot configurations considered for this study, corresponding to the dimensions listed in Table III for circle and square plots with the same areas. Cluster plot dimensions are shown for the nominal USFS FIA subplot (circle) dimensions and equivalent area square subplots. Red polygons represent actual field plot shapes used in this study.

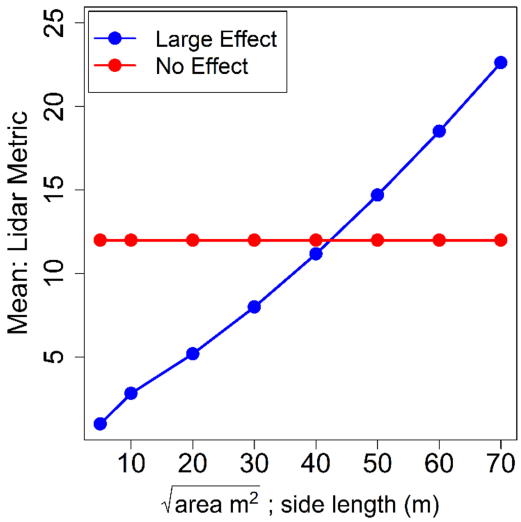

Fig. 5. Schematic of two hypothetical lidar metrics, one with a large change of spatial support effect on the mean (blue) and the other with no change of spatial support effect on the mean (red).

of lidar metric means (the population mean $\mu_{\bar{x}}$ from 10 000 virtual plots) due to the effects that arise from differences in support areas

$$\text{eCV}\% = \frac{\sigma_{\bar{x}}}{\mu_{\bar{x}}}\ 100\% \tag{1}$$

where $\sigma_{\bar{x}}$ is the standard deviation of the lidar metric's means across plot sizes and $\mu_{\bar{x}}$ is the mean of lidar metric means for multiple plot sizes.

G. Model Fitting

Ordinary least squares regression was used in this study to model the relationships between field measurement derived forest attributes and auxiliary remote sensing attributes. Models were then used with auxiliary remote sensing information to make predictions of forest attributes both for the entire target population (10 000 virtual plots) and for sample plots. Forest attribute predictions were generated to support inferences about both prediction (e.g., maps) and estimation (e.g., the population mean). Models were fit for each of the plot designs: cluster plots, subplots, and large plots, although subplot attributes were aggregated to the cluster-plot level for estimation purposes.

In a study such as this one involving many variables, considerable effort is often needed to select a subset of the many potential auxiliary variables. Our objective was to select predictors that explained as much variation as is feasible, without overfitting the training data or demonstrating lack of fit. We first performed an exploratory exercise for multiple regression using automated variable selection. This helped to identify groups of variables that work effectively in combination. Automated variable selection in this study was performed with the leaps and bounds algorithm [30] implemented in the "leaps" package [31] for the *R* statistical programming language [29]. Various models selected by the algorithm and their component variables were then evaluated for predictive power, correlation with each other, and generality in predictions across forest attributes. Finally, a "fixed" set of variables was selected with expert interpretation. Specific findings for variable selection are described in greater detail in the results.

Inferences about model performances use root mean square error (RMSE) and coefficient of determination (R^2)

$$\begin{aligned}\text{RMSE} &= \sqrt{\frac{\sum_{i\in s} {e_i}^2}{n}} \\ \text{RMSE}\% &= \frac{\text{RMSE}}{\bar{y}} \times 100\% \\ R^2 &= 1 - \frac{\sum_{i\in s}\left(y_i - \hat{y}_i\right)^2}{\sum_{i\in s}\left(y_i - \bar{y}\right)^2}\end{aligned} \tag{2}$$

y_i is a forest attribute (e.g., BA) on plot *i*.
$\hat{y}_i$ is a model prediction of y_i.
$\bar{y}$ is the sample mean.

H. Estimation

This section describes estimation of forest attributes with and without auxiliary lidar information. Estimation for a simple random sample (SRS) without auxiliary information serves as a benchmark for estimation performance, a common practice in survey sampling. Estimation of forest attributes with lidar auxiliary information is implemented through an approach called "model-assisted" estimation [32]. In model-assisted estimation, a model is used to relate a "y" variable (e.g., forest attributes) to auxiliary "x" variables (e.g., lidar metrics), to "assist" in estimation of population attributes. Model-assisted estimation is described in greater detail later in this section. For subplot estimation inferences, models were first fit at the subplot scale, and then results were aggregated to the plot scale for estimation.

Our reference for estimation with a SRS with no auxiliary information is the sample-mean estimator of the population mean

$$\bar{y} = \frac{\sum_{i\in s} y_i}{n} \tag{3}$$

where s is a SRS composed of n observations taken from a population of size *N*, and y_i is a forest attribute (e.g., BA) measured on plot *i*.

The mean squared error (MSE) of $\bar{y}$ is the expected variation of the sample mean around the population mean, which is equal to its variance $V(\bar{y})$ plus its squared bias $B(\bar{y})^2$

$$\begin{aligned}\text{MSE}\left(\bar{y}\right) &= E\left[\left(\bar{y} - \mu_y\right)^2\right] \\ &= V\left(\bar{y}\right) + B(\bar{y})^2.\end{aligned} \tag{4}$$

Since $\bar{y}$ is unbiased for μ_y, its MSE is simply its variance

$$\text{MSE}\left(\bar{y}\right) = V\left(\bar{y}\right).$$

For a large *N* and small *n*, we estimate $V(\bar{y})$ from the sample variance S_y^2

$$\hat{V}\ \left(\bar{y}\right) = \frac{S_y^2}{n}. \tag{5}$$

1) Model-Assisted Estimation: A model-assisted population mean estimator for a SRS when there is no change in spatial support is

$$\hat{\mu}_{\text{MA},0} = \frac{\sum_{j\in I}\hat{y}_j}{N} + \frac{\sum_{i\in s} e_i}{n} \tag{6}$$

where $e_i = y_i - \hat{y}_i$, and $\hat{y}_i$ is the prediction for element i. The absence of change in support is indicated by subindex 0 in $\hat{\mu}_{\text{MA},0}$. In the context of this study, our population is $N = 10\,000$ virtual plots. Since $\hat{\mu}_{\text{MA},0}$ is approximately unbiased for μ_y, its bias term may be omitted

$$\begin{aligned}\text{MSE}\ (\hat{\mu}_{\text{MA},0}) &= V\left(\hat{\mu}_{\text{MA},0}\right) + B(\hat{\mu}_{\text{MA},0})^2 \\ &\approx V\left(\hat{\mu}_{\text{MA},0}\right)\end{aligned} \tag{7}$$

with estimator

$$\begin{aligned}\hat{V}\left(\hat{\mu}_{\text{MA},0}\right) &= \frac{S_e^2}{n} \\ S_e^2 &= \frac{\sum_{i\in s} e_{i,0}^2}{n}.\end{aligned} \tag{8}$$

For change of spatial support, the estimator receives a subscript Δ, e.g., $\hat{\mu}_{\text{MA},\Delta}$. Considering the potential bias from change of spatial support, $B(\hat{\mu}_{\text{MA},\Delta})$, we estimate $\text{MSE}(\hat{\mu}_{\text{MA},\Delta})$ as

$$\begin{aligned}\widehat{\text{MSE}}\left(\hat{\mu}_{\text{MA},\Delta}\right) &= \hat{V}\left(\hat{\mu}_{\text{MA},\Delta}\right) + \hat{B}(\hat{\mu}_{\text{MA},\Delta})^2 \\ \hat{B}\left(\hat{\mu}_{\text{MA},\Delta}\right) &= \hat{\mu}_{\text{MA},0} - \hat{\mu}_{\text{MA},\Delta}\end{aligned} \tag{9}$$

where $\hat{V}(\hat{\mu}_{\text{MA},\Delta})$ is calculated in the same way as $\hat{V}(\hat{\mu}_{\text{MA},0})$, but using residuals from the model fit with a change of spatial support.

Typical model-assisted forest inventory applications do not include a bias term for shape or size mismatch (Δ). It is simply assumed that prediction errors for model training plots are representative of the error distribution for predictions to grid cells—an assumption that may not be accurate.

2) Efficiency Estimation: We use relative efficiency (RE) to characterize sampling efficiency for various estimation strategies (8). RE has a convenient practical interpretation: it is the multiple of the SRS size (n) needed for the SRS $\bar{y}$ estimator to be as efficient as some alternative estimator, in this case, a model-assisted estimator. For example, a RE of 2.0 for the model-assisted estimator means that twice as many plots are needed with the $\bar{y}$ estimator to be as efficient (achieve the same standard error) as the model-assisted estimator.

Model-assisted and SRS $\bar{y}$ estimators were compared for a fixed and matched sample size using

$$\text{RE}_n = \frac{\hat{V}\left(\bar{y}\right)}{\text{MSE}_{\hat{\mu},\Delta}}. \tag{10}$$

RE does not usually depend on n, but since $\hat{\mu}_{\text{MA},\Delta}$can be a biased estimator, the magnitude of RE is dependent on sample size. For the purposes of this study, we used RE_{200}, i.e., RE when we set $n = 200$. It is worth noting that as n increases, $\text{MSE}_{\hat{\mu},\Delta}$ does not go to zero when $\hat{B}(\hat{\mu}_{\text{MA},\Delta})^2 > 0$, while $\hat{V}(\bar{y})$ does go to zero. This means that when change of spatial support bias is present, the RE of biased model-assisted approaches will decrease for increased sample sizes.

III. Results

A. Effects of Plot Shapes and Sizes on Lidar Metrics

The results in Fig. 6 demonstrate that lidar metric values may change dramatically (many-fold) for different plot areas, depending upon the choice lidar metric. For example, changes in median height (htP50) are largely ignorable, while mean voxel volume (voxVol) varied from less than 1.0 m^3 to approximately 150 000 m^3 for the smallest and largest plot areas respectively. The lidar metrics that were insensitive to plot area in Fig. 6 also had corresponding low eCV% values, where eCV% is a numerical score proposed for sensitivity to changes in spatial support. The eCV% values for all lidar metrics considered in this study are provided in Appendix 2 Table V.

From Fig. 6, we can also make some inferences about the effects of plot shapes on lidar metric values. Most importantly, the effect of circle versus square plots appears to be totally ignorable. The lack of circle versus square shape effects is fundamental to defensible inferences for most ABA forest inventories with lidar, because most field plots are circular, and most grid cells are square. This finding suggests that pairing circular plots with square grid cells is perfectly acceptable in practice and will not introduce biases. Because of the strong evidence that circle and square plots are interchangeable, the remaining results are presented only for circular plots with square grid cells.

In contrast to the effects from circle versus square plots, use of cluster plots had the potential to introduce large biases. Lidar metrics computed from cluster plots appear to behave like much larger-in-area circle or square plots.

The biases in lidar metrics caused by differences between plots and grid cells are compared for plot-clip and raster-intersect approaches in Fig. 7. Both plot-attribution approaches had appreciable nonzero biases for all lidar metrics for 5 m and 10 m grid cells. The magnitudes of biases for the raster-intersect approach fell below 2% for every lidar metric with grid cells 20 m or larger. Differences between the three plot footprints considered (Cluster, Subplot, and Large) were less than 1 percentage point for the raster intersect approach. Biases for the plot-clip approach were generally larger than those for the raster-intersect approach and differences between plot footprints were more pronounced for the plot-clip approach.

The variation observed for some of the lidar in Fig. 6 suggests that differences between plot and grid cell sizes are likely to cause biases in ABA lidar forest inventory. This finding is further supported by the metric biases reported in Fig. 7 for departures from the original plot sizes. Using circular plots with square pixels of equal areas (as is common practice; Fig. 6) does not appear to cause bias. In contrast, cluster plots provide added complication because they do not behave like grid cells with corresponding area.

B. Effects of Plot Attribution Method on Variable Selection by Plot Type

The results in Table IV provide insight into variable selection and relative predictive power as a function of plot attribution method (point clip versus raster-intersect), as well as insight into their sensitivity to plot shape. While the raster-intersect approach

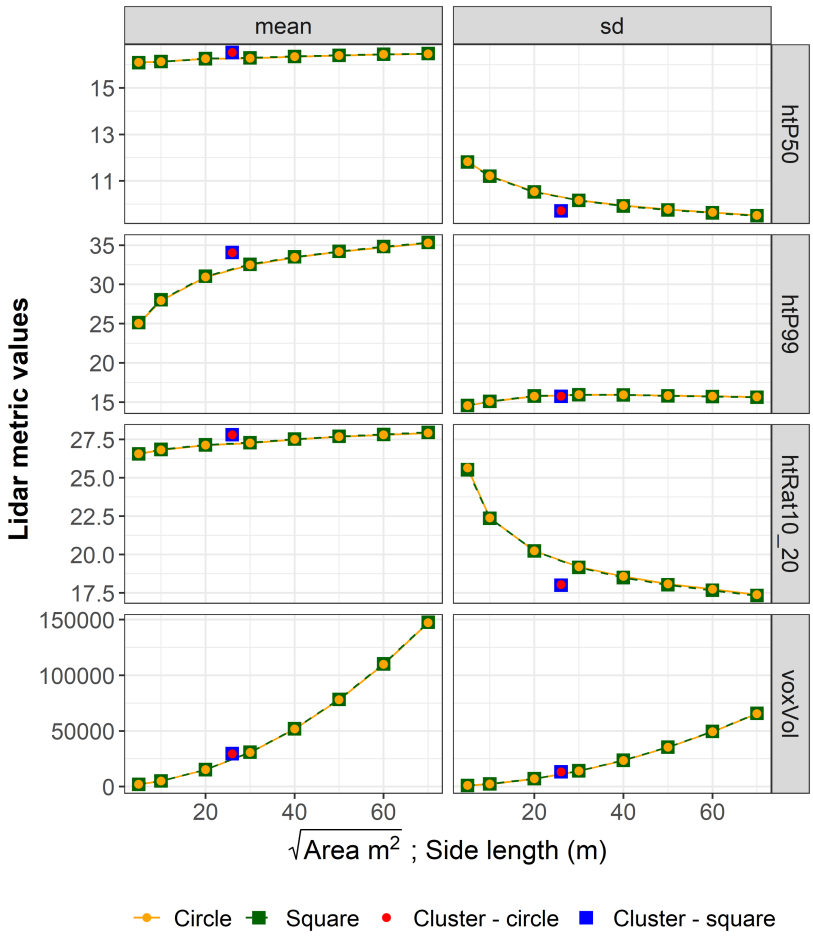

Fig. 6. Means and standard deviations (sd) of lidar metrics from 10 000 virtual plots relative to grid cell area ($\sqrt{\text{area } m^2}$) or the side length. Units are meters for htP50 and htP99, percent (%) for htRat10_20, and cubic meters for voxVol. Cluster plot results are shown for the observed size with both circle and square subplots to demonstrate the differences associated with this plot shape. eCV% scores for these lidar metrics are 0.86 for htP50, 11.37 for htP99, 1.74 for htRat10_20, and 96.12 for voxVol.

was the least sensitive to change of spatial support effects in the previous section, the raster-intersect approach consistently explains less variation on average than the plot-clip approach. This was both with automated variable selection and using a fixed set of predictors.

The variables selected with automated variable selection appear to be clustered primarily by forest attribute. Otherwise, the plot attribution approach often yields quite different sets of variables within the same plot type and forest attributes. Large plots are partly an exception to this, with similar sets of variables between attribution methods in some instances. The variable scaled voxel volume (voxVolScl) was selected into 21 top models, which is twice as many models as the next most common metric, scaled surface ares (srfAreaScl).

The magnitude of the effect of attribution method (point-clip versus raster-intersect) was smallest for models fit with subplots. Point-clip and raster-intersect approaches were often within one percentage point for subplots using the fixed model. It is cautioned that Table IV should not be used to compare plot types directly, especially large plots with either cluster or subplots, due to confounding factors such as edge effects [33] and aggregation to different plot areas [34].

C. Change of Spatial Support Effects on Estimation

Model-assisted estimation biases and relative efficiencies are provided for both plot-clip and raster-intersect approaches. Recall that in the point-clip approach, plots are attributed with lidar metrics computed for the plot footprints, while prediction and estimation use raster grid cells which may differ in size and shape from the plot footprints. With the raster intersect approach, in contrast, identical grid cells are used both for plot attribution and for prediction and estimation. For the purpose of estimation with subplots, models were fit to subplots and then averaged by plot for estimation.

All of the models fit for estimation used the same fixed group of lidar metric predictors including: htP10, htP90, cover1, and htRt10_20. The selected lidar metrics are fairly typical in ABA analyses and are easy to compute with a variety of software tools used to process lidar for forestry applications. These lidar predictors are also weakly correlated with each other, which avoids collinearity issues, and they predict reasonably well for a wide range of scenarios. We would not necessarily use this exact set of variables for all of the forest attributes in practical applications, but the approach removes variable selection as a

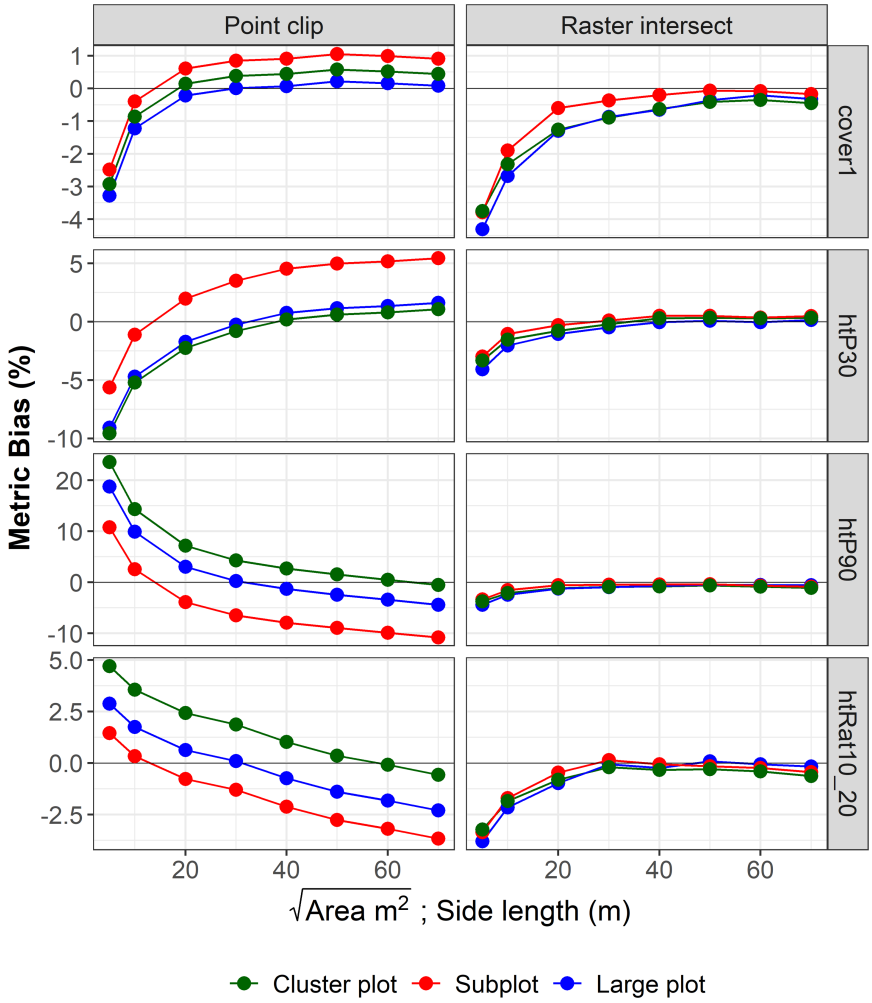

Fig. 7. Grid cell based lidar metrics biases relative to plot-based lidar metrics by attribution approach for 10 000 virtual plots. Results are for circular plot footprints relative to square grid cells.

confounding effect in characterizing effects of change of spatial support. We initially experimented with results from automated variable selection, but the resulting models were highly unstable (unusually high or low predictions for at least some observations), and often included variables which resulted in dramatic scale mismatch related biases. Automated variable selection can be an effective as an exploratory tool, but analyst intervention is needed for reasonable final variable selection.

From Fig. 8, we can see that model-assisted estimation with the point-clip approach is biased for nearly all of the grid cell sizes, and by as much as 15% . Estimation with large-plots and subplots were unbiased for grid cells that matched their corresponding plot areas. Cluster plots were approximately unbiased for 60 m grid cells, which have much greater area than the cluster plots but cover a similar spatial footprint. The raster-intersect approach, in contrast, was unbiased for nearly all of the grid cell side lengths, with the exception of grid cells that were dramatically smaller in area than the plot size.

As with the results for bias, the result for model-assisted relative efficiency (RE) in Fig. 9 suggest that the plot-clip approach is highly sensitive to disagreement between plot size and grid cell size. If the plot size and shape closely match the grid cell size, the plot-clip approach yielded the best (highest) efficiency, and declined rapidly for departures from matched plot and grid cell areas. Cluster plots, in contrast, were most efficient for 70 m grid cells, the largest grid cell size that was tested.

The results for raster-intersect, in contrast to the plot-clip approach, were much less sensitive to grid-cell size. Large plots and subplot efficiencies peaked at around 20 m grid cells and declined gradually towards 70 m. Cluster plot relative efficiencies were the least sensitive to grid cell size of the three plot designs, being fairly constant between 20 and 70 m.

The results presented in this section for bias and efficiency for the point-clip approach are highly sensitive to the choice of predictor variables. The results in this section are demonstrative only, and an alternate set of variables may result in greater or less effect from change in spatial support.

IV. Discussion

A. *Point-Clip Approach*

The results from this study suggest that the point-clip approach, the typical area based approach (ABA) to forest inventory with auxiliary lidar, can be highly sensitive to changes

TABLE IV
OLS MODEL PERFORMANCES FOR BOTH POINT-CLIP ("CLIP") AND RASTER-INTERSECT ("INTERSECT") APPROACHES

			Fixed		Auto VS		
y	plot	method	R^2	RMSE %	R^2	RMSE %	*Auto VS:* best-model predictors
BA	cluster	clip	0.56	32.2	0.65	28.6	eig2; voxVolScl; xyzMnRtScl; htP10
BA	cluster	intersect	0.49	34.7	0.56	32.0	curv; hznlty; voxVolScl; xySdRtScl
BA	large	clip	0.67	34.3	0.74	30.5	srfAreaScl; voxVolScl; xMin; htP80
BA	large	intersect	0.60	37.8	0.67	34.4	srfAreaScl; voxVolScl; htMn; htP30
BA	subplot	clip	0.57	31.8	0.65	28.7	srfAreaScl; voxVolScl; zRat10; zRat30
BA	subplot	intersect	0.56	32.1	0.62	29.9	grdVolScl; voxVolScl; xyzMnRt; xyzMaxRtScl
C	cluster	clip	0.60	36.6	0.68	32.9	lnrty; voxVolScl; xyCvRtScl; htP80
C	cluster	intersect	0.56	38.7	0.59	37.3	eig1; sphrcty; voxVolScl; xySdRtScl
C	large	clip	0.67	40.1	0.74	36.0	srfAreaScl; zIQ; htMn; htP20
C	large	intersect	0.60	44.5	0.68	39.4	srfAreaScl; htMn; htP20; htP60
C	subplot	clip	0.63	35.5	0.68	33.1	srfAreaScl; voxVolScl; zIQ; htP50
C	subplot	intersect	0.64	35.2	0.67	33.6	grdVolScl; voxVolScl; zCvScl; htP70
QMD	cluster	clip	0.60	21.2	0.67	19.2	areaCover; xyzCorScl; xyzSdRt; htMn
QMD	cluster	intersect	0.55	22.4	0.6	21.1	areaCover; zCv; htP70
QMD	large	clip	0.63	24.8	0.7	22.4	areaCover; xyzMnRtScl; htMnScl; htP80
QMD	large	intersect	0.58	26.5	0.64	24.6	eig3; plnrty; xRatHt; ySd
QMD	subplot	clip	0.61	24.5	0.62	24.2	voxVolScl; xyzSdRt; zIQ; htP40
QMD	subplot	intersect	0.62	24.3	0.65	23.3	voxVolScl; xyzSdRt; htP20; htP99
SDI	cluster	clip	0.43	33	0.52	30.3	voxVolScl; xyCvRt; xySdRt; yMin
SDI	cluster	intersect	0.36	35.2	0.45	32.7	eig1; voxVolScl; zIQScl; htP40
SDI	large	clip	0.52	36.7	0.52	36.7	xyzMinRt; xyzMnRt; yMin; xyzMaxRtScl
SDI	large	intersect	0.46	38.9	0.46	39.1	xyzMinRt; xyzMnRt; yMin; xyzMaxRtScl
SDI	subplot	clip	0.48	31.2	0.57	28.6	voxVolScl; xMin; zRat10; xyzMaxRtScl
SDI	subplot	intersect	0.48	31.4	0.5	30.8	curv; eig1; zRat10; xyzMaxRtScl
TPH	cluster	clip	0.49	41	0.55	38.5	areaCover; htRat10_20; htP10; xyMnRtScl
TPH	cluster	intersect	0.42	43.9	0.47	41.9	eig1; grdVolScl; xyzSdRt; htRat10_20
TPH	large	clip	0.49	42.2	0.31	49.3	xyzSdRt; htRat2_4; zRat20; xyzMaxRtScl
TPH	large	intersect	0.40	45.8	0.43	44.7	srfAreaScl; htRat2_4; htMnScl; htP50
TPH	subplot	clip	0.46	41.9	0.53	38.9	areaCover; xyzCvRt; htRat10_20; xyzMaxRtScl
TPH	subplot	intersect	0.41	43.7	0.44	42.6	eig1; xyzSdRt; htRat10_20; xyzMaxRtScl
VOL	cluster	clip	0.67	34.6	0.74	30.5	grdVolScl; hznlty; voxVolScl; htP80
VOL	cluster	intersect	0.62	37	0.66	34.7	eig1; voxVolScl; xySdRtScl; htRat10_20
VOL	large	clip	0.71	38.8	0.78	33.5	srfAreaScl; voxVolScl; htMn; htP20
VOL	large	intersect	0.64	43.1	0.72	38.0	srfAreaScl; voxVolScl; htMn; htP20
VOL	subplot	clip	0.71	32	0.76	29.3	srfAreaScl; voxVolScl; zIQ; htP50
VOL	subplot	intersect	0.70	32.3	0.73	30.8	voxVolScl; xyzCvRt; zCv; htP70
mean of clip			**0.58**	**34.02**	**0.63**	**31.73**	
mean of intersect			**0.54**	**35.97**	**0.59**	**33.94**	

* Models were fit with automated variable selection ("Auto VS") and with a fixed set of lidar metrics. The fixed model included htP10, htP90, cover_1, and htRt10_20. Subplot residuals are averaged by cluster plot to compute R^2 and RMSE% values. BA: basal area, C: carbon, QMD: quadratic mean diameter, SDI: stand density index, TPH: trees per hectare, Vol:bole volume.

of spatial support, or differences between the sizes and shapes of plots relative to raster grid cells. This may introduce biases that practitioners should be careful about. However, as was also demonstrated by Packalen et.al. [16], the use of circular plots with square pixels of the same area does not appear to introduce noticeable effects. To eliminate biases associated with differences in spatial support, the area of the grid cell must match the area of the plot, and the plots and grid cells must have compatible shapes. As far as we can tell, this makes the cluster plot design that we explored incompatible with traditional ABA lidar inventory (the point-clip approach), unless models are developed at the subplot scale and applied (predicted) to raster grid cells with the same areas as the subplots. Processing lidar using cluster-shaped grid cells and stored in square pixels would be a potential alternative for cluster plots, but it is not one supported by any point cloud processing tools that we are familiar with.

Our findings suggest that care should also be taken in the use of lidar-derived raster grid cell metrics. Raster derivatives of lidar point clouds are commonly deployed alongside forest attribute predictions by forest management organizations. For example, lidar height quantiles and cover metric rasters may be deployed as part of GIS resources. In using these layers, users should be aware that the values can be dependent upon grid cell sizes: upper canopy heights from fine grid cells (e.g., 5 m) may be as much as 10 m different from coarser grid cells (e.g., 70 m), painting very different pictures of the forest conditions if their relative spatial dependencies are not recognized. Measures of cover and other ratio-based metrics, in contrast, appear to be more robust to differences in grid cell sizes.

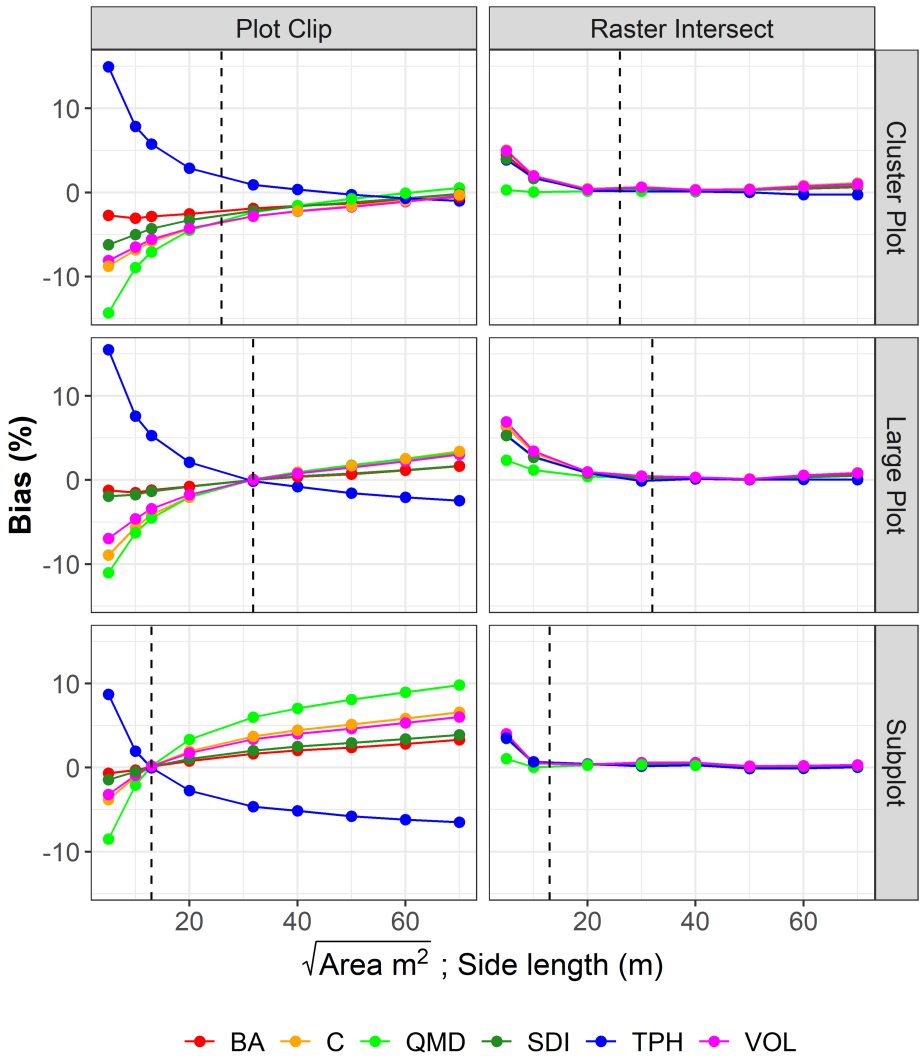

Fig. 8. Percent biases (Bias %) for model-assisted estimates with *point-clip* and *raster-intersect* approaches relative to plot or grid cell areas ($\sqrt{\text{area } \boldsymbol{m}^2}$), or the equivalent side length of grid cell. Dashed vertical lines represent corresponding plot areas ($\sqrt{\text{area } \boldsymbol{m}^2}$) used to fit OLS models. For subplots, models were fit to individual subplots and then predictions and errors were averaged by cluster plot. BA: Basal area, C: Carbon, QMD: Quadratic mean diameter, SDI: Stand density index, TPH: Trees per hectare, Vol: Bole volume.

The study by Packalen et.al. [9] is the only example outside of our study we are aware of that investigates changes in spatial support issues in the context of ABA lidar forest inventory. Our findings with respect to the point-clip approach to ABA forest inventory differ from those observed by Packalen et.al. [9] in that they did not encounter deleterious effects from changes in spatial support. In contrast, we observed biases approaching 15% and dramatic differences in efficiency resulting from change of spatial support. The lack of agreement between our findings and those from Packalen et.al. [9] may be explainable by a number of factors including different tree sizes (our average trees are approximately three-fold the size of those in boreal forests of Finland), different ranges of grid cell sizes (5–70 m here versus 12.5–25 m), and different spatial extents (14 000 km^2 here versus 1000 ha). Differences in choices of variables between our two studies may also play a role in our different results as we observed dramatic differences from using different lidar metrics (results not included).

B. *Raster-Intersect Approach*

The raster-intersect approach is a promising alternative to the typical (point-clip) ABA lidar approach, which appears to reduce or eliminate biases related to changes in spatial support for the scenarios explored here. The raster intersect approach is also much more flexible than the point-clip approach enabling (approximately) unbiased estimation even with cluster plots. However, estimation biases were still present with the raster-intersect approach when used with very small grid cells relative to the field plots. The best results for the raster-intersect approach were also slightly less efficient than the best results for point-clip approach.

There is another spatial mismatch problem identified by Réjou-Méchain et.al. [35], which has the potential to negatively affect the raster-intersect approach. The potential problem arises when the raster grid cell is so much larger than the field plot that the correspondence between field measurements and lidar

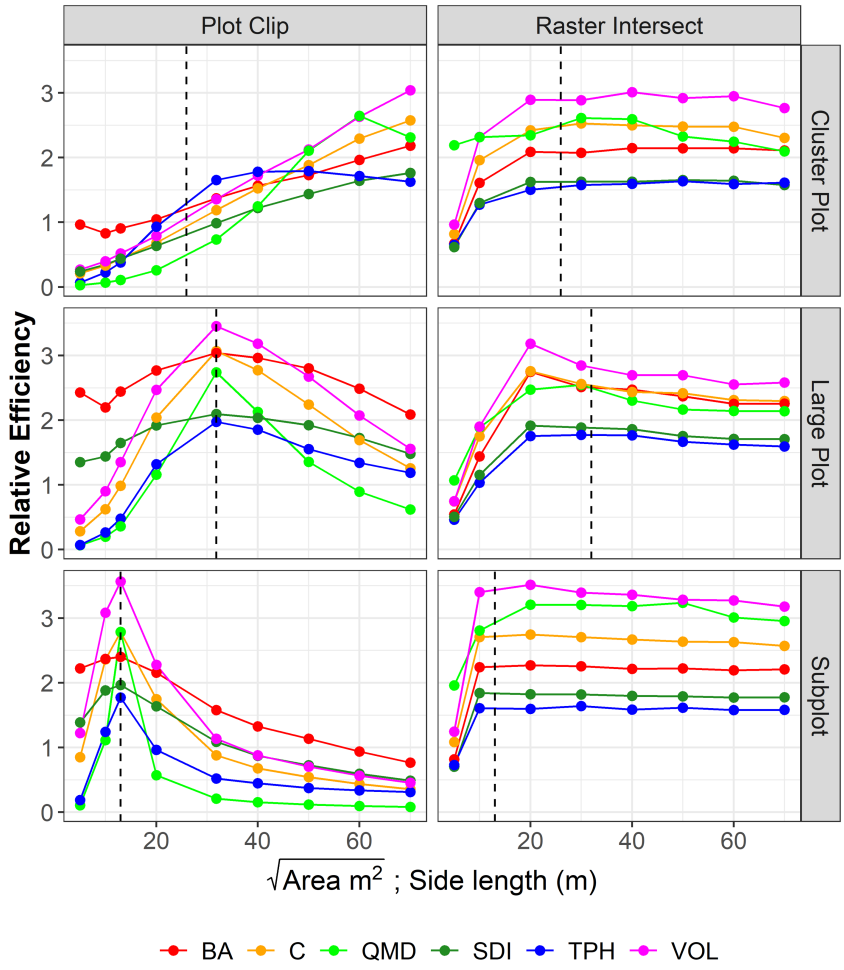

Fig. 9. Relative efficiencies for model-assisted estimates with *point-clip* and *raster-INTERSECT* approaches relative to plot or grid cell areas ($\sqrt{\text{area } \boldsymbol{m}^2}$), or the equivalent side length of grid cell. Dashed vertical lines represent corresponding plot areas ($\sqrt{\text{area } \boldsymbol{m}^2}$) used to fit OLS models. For subplots, models were fit to individual subplots and then predictions and errors were averaged by cluster plot. BA: Basal area, C: Carbon, QMD: Quadratic mean diameter, SDI: Stand density index, TPH: Trees per hectare, Vol: Bole volume.

metrics declines. Fortunately, we did not observe this effect in the range of 5–70 m grid cells. However, clearly even with the raster-intersect approach, plot and grid cell shapes and areas should still be matched as closely as possible.

C. Modifiable Areal Unit Problem

The MAUP is concerned with how inferences vary for different spatial scales or for different polygons sizes and shapes used for aggregation. Although we do not emphasize MAUP here, our study relates to the MAUP in that we aggregate lidar points and raster grid cells for different plot and grid cell areas (25–4900 m^2) and different shapes (circle, square, and cluster). We found that using a cluster plot shape had a noticeable effect on ABA forest inventory with lidar that was distinct from plot area. Aggregation with circle versus square plots, in contrast, did not have a noticeable effect. Our results also indicated that large circular plots were less susceptible to COSPs than cluster plots or subplots and that cluster plots behave like a much larger contiguous region. Finally, we demonstrate that variable selection appears to be fairly robust to plot sizes and shapes; the same group of predictors perform similarly for each forest attribute regardless of plot size and shape. We are not aware of any other studies or journal publications, which address change of spatial support as a function of area size and shape in the context of ABA lidar forest inventory. Although our studies are related, unlike Ozkan and Demirel [24], this study was not suited to evaluate model performance as a function of plot types or sizes.

D. Bias Reduction or Avoidance With the Point-Clip Approach

The simplest way to avoid COSPs with ABA lidar forest inventory is to use circular field plots with the same areas as raster grid cells. This approach does not work well with cluster plots because cluster plots were biased for corresponding grid cell areas. Alternatively, we found that unbiased estimation was feasible for cluster plots with the point-clip approach if we fit models to subplots and predict for grid cells that matched the subplot areas. However, we find the rigidity of the point-clip approach to be unsatisfying as it locks the analyst to matched field plot and grid cell sizes. This can result in multiple practical issues. One issue is that for large pixels field plots would be too large and expensive to measure, e.g., 34 m radius field plots are

needed to match 30 m grid cells. Another related issue is that raster grid cells may be too small or awkward if matched to a particular plot size, e.g., 14.2 m grid cells to match 8 m radius circular plots.

An alternative approach that would not require exactly matching plot and grid cell shapes is to use lidar metrics, which are less sensitive to change of spatial support effects.

Table V can be used to aid in selection of robust lidar metrics: metrics with smaller eCV% scores are less affected by changes in spatial support. Metrics such as the mean and median and ratio metrics are less susceptible to change of spatial support effects. A downside of this approach is that only using metrics, which are robust to spatial effects may reduce the explanatory potential of lidar predictors.

E. Alternative Plot Attribution Methods

There are several related plot-attribution methods that deserve further attention, but which we were unable to explore in this study. The first approach is to use the raster-intersect approach with a single raster grid cell (the approach evaluated in this study uses an area weighted mean of lidar grid cells). This is the approach currently used by USFS FIA for post-stratification and has the benefit of exactly matching the spatial support between model fit and prediction datasets. However, its potential to explain variation may be greatly reduced over the methods used in this study. In the single-pixel variation, the grid cell may poorly overlap the plot (e.g., the plot center lands in a grid cell corner), the shape of the plot may differs greatly from the grid cell (e.g., cluster plots and square grid cells), or the grid cells may be much smaller than the field plots (e.g., 5 m grid cells and 30 m plots).

Another variation on the raster-intersect approach is to build a set of grid cells in the vicinity of each field plot where the centermost pixel is centered on the field plot. This would maximize intersection between the central pixel and the field plot. This could be used both for an area-weighted intersection as used here, or in the single-pixel variation discussed above. The improvement would be most notable for grid cell sizes approaching or exceeding single circular plot areas as they would maximize the overlap between a single pixel and a plot, potentially increasing the efficiency of the raster-intersect approach.

While the raster-intersect approach is approximately unbiased for some grid cell sizes, scales finer than the plot size are still biased. This is because many small grid cells are averaged for each individual plot, similar to having a moving window centered on each plot. This suggests another approach using a moving window average applied to the fine-resolution target raster where the window is based on the size and shape of the field plot. The "plot-smoothed" fine-scale raster would then be used both to attribute field plots and for predictions. This approach may eliminate biases observed for small raster cells.

F. Study Limitations

A limitation of this study is the use of a single fixed set of lidar metrics for estimation. In practice, the best lidar metrics will vary by forest attribute and may vary for differences in plot size, attribution approach, and even sample. Unfortunately, automated variable selection provides potential for confounding inferences about change of spatial support effects. The use of a single set of variables is not a perfect solution, but it is a reasonable compromise between practicality and demonstrating potential effects of changes of spatial support. In preliminary results (not reported here), we found that change of spatial support effects were dramatically worse when variables were selected automatically, e.g., with the leaps and bounds algorithm [30]. This is motivation to use automated variable selection only for data exploration.

V. Conclusion

Our findings show that differences between plot and raster grid cell sizes and shapes (or, more broadly: "change of spatial support") can result in large biases in ABA lidar forest inventories. The biases arose primarily when the plot footprints clipped from lidar point clouds (the "plot-clip" approach) diverged greatly from grid cells. There was also considerable bias in using cluster plots with equal-in-area raster grid cells. However, no bias was observed when using circle plots with square grid cells of the same areas.

Fortunately, biases from changes of spatial support in ABA lidar forest inventory can be largely avoided or mitigated by:

1) matching plot and pixel areas (excluding cluster plots);
2) using lidar metrics, which are robust to changes in spatial support; and
3) by attributing field plots directly from raster grid cells (the "raster-intersect" approach).

Although the point-clip approach achieved slightly higher efficiency than the raster-intersect approach in the best cases, the raster-intersect approach is considerably more flexible than the point-clip approach and sacrifices minimal efficiency. The raster-intersect approach was also the most reliable for use with cluster plots.

Acknowledgment

The authors would like to thank the USDA Forest Service Region 6 and the Pacific Northwest Forest Inventory and Analysis program for collecting and compiling the data used in this study. The authors would also like to thank Natalia Malaga for her feedback on analyses and on an early draft.

Appendix 1
Glossary

ABA—Use of areas or regions (commonly plots and grid cells) to infer properties of a population. In the context of forest inventory with auxiliary lidar, this includes models fit between *field plot measurements* and lidar plot measurements, then predictions for each grid cell in the target population.

Airborne laser scanning (ALS)—An integrated system of scanning (typically) *lidar* sensor, *GNSS*, and inertial measurement unit that is mounted on an airborne platform and used to measure terrestrial features.

Cluster plot—A field plot composed of multiple spatially independent subregions or "subplots."

Design effect—The ratio of the estimated sampling variance associated with a *SRS* mean relative to some alternative estimation strategy. The inference is the ratio of sampling intensity needed with an SRS mean to achieve the precision of an alternate estimation strategy. For example, a design effect of 0.5 means that half as many plots from the alternative design are needed for to be as precise as estimation with the SRS sample mean $\bar{y}$ estimator.

Efficiency—The ratio of sampling variation relative to sample size, which is a concept that is not strictly associated with a particular statistic but is commonly inferred from RE or *design effect*.

Change of *spatial support*—Differences in the spatial properties of measurements (e.g., different grid cell sizes or orientation or differences in plot shapes) which can affect the properties of a distribution of measured values. For example, upper lidar height percentiles (e.g., 95 percent) computed for 5 m grid cells are expected to be smaller on average than for 30m grid cells. This term is often used interchangeably with "change of support" in the geostatistical literature—also closely related to the *MAUP*.

Field plot—the point, line, or area associated with in-the-field measurements of the environmental or vegetation conditions, typically associated with a measurement protocol and spatial sampling design. For *ABA* lidar forest inventory, a field plot is typically a precisely georeferenced circular area distributed in some way (e.g., purposively, on a grid, randomly, or proportional to some covariate) across the target population.

Global Navigation Satellite System (GNSS) receiver (survey grade)—an instrument that uses signals received from constellations of satellites for positioning, colloquially referred to as "GPS," which is the American system for GNSS positioning. A survey-grade GNSS receiver is one defined as achieving 2 cm accuracy in the open, a specification that typically requires differential correction against a known base station.

Grid cell—an approximately square (typically) region, typically one of a series of gridded such regions associated with corresponding measurement information and stored in a digital raster file format such as a geotiff. For example, a raster representation of data stored for 30 $\times$ 30 m grid cells is commonly described as a "30 m raster."

High Performance GNSS (HPGNSS)—a standard used by FIA based on in-the-forest positioning accuracy (1 m horizontal *RMSE* and 95% of horizontal errors $<$2 m) and is commonly determined by field protocol (height, data collection rate, occupation duration) and GNSS receiver quality (typically survey-grade).

ITD—the practice of basing landscape inferences on individual trees detected from lidar or imagery. This is a common alternative *ABA* inferences from lidar, or may serve as an input to ABA inferences.

Lidar—Light detection and ranging, the fundamental technology which enables *ALS*; "lidar" is also used as a more generic naming convention for ALS.

Lidar metric—a statistic computed on the attributes of a *lidar* point cloud, in the context of this study, typically with the intention to characterize structural vegetation properties, but may also include topographic or spectral properties associated with individual points.

MAUP—the phenomenon that inferences made at different spatial scales or using different sets of polygons for aggregation can result in different inferences about individual attributes and the relationships between attributes—a concept closely related to the COSP.

Pixel (spatial raster)—in the context of this study, a "pixel" refers to a "picture element," the digital representation of information collected for an approximately square horizontal region (see "*grid cell*") and stored in a "*raster*" file format containing matrix of such pixels for an area.

Plot—see "Field plot."

Point-clip approach—a plot attribution method that uses lidar points clipped from the spatial region which exactly matches the plot footprint to compute lidar metrics from plots. This is an alternative to the *raster-intersect approach*.

Raster—a digital representation of grid cells commonly stored in two-dimensional arrays of values.

Raster-intersect approach—a plot attribution approach that uses *grid cell* values stored in a *raster* layer and assigns them to a plot based on their spatial intersection. This is an alternative to the *point-clip approach*.

RE—the ratio of the estimated sampling variation of some design paired with an estimator relative to the estimated sampling variation of the simple random $\bar{y}$ sample mean estimator of the population mean. RE is the inverse of *design effect***,** where a RE larger than 1.0 indicates that the alternative design is more efficient than the SRS $\bar{y}$ estimator.

RMSE—the square root of the mean squared deviation associated with some prediction process, e.g., the mean of squared deviations between observed and predicted values from ordinary least squares regression for a collection of sample plots.

Sample frame—the manner in which the target population is characterized to facilitate sampling. For example, in forestry the sample frame is often the 2-dimensional space occupied by the target forest. A sample of the region is then composed of field plots distributed spatially across the 2-dimensional space.

SRS—a process of selection in which every element in *the sample frame* has equal probability of selection and where each sample element is completely independent of every other element.

Spatial support—the properties of spatial objects such as type (e.g., point, polygon, and grid cells), size, shape, and orientation, which may affect values and distributions of attributes of interest including auxiliary variables.

Standard error—a sample-based estimate of the sampling variation (standard deviation) of a statistic, commonly estimated for means and totals, e.g., "the standard error of the mean" is the estimated variation associated with a mean estimator and sampling strategy.

Tesselate—to divide an entire spatial domain into nonoverlapping shapes without any gaps, for example, with a regular grid of square or hexagonal cells.

APPENDIX 2
SUMMARY OF LIDAR METRIC SENSITIVITY TO PLOT OR GRID CELL SIZE EFFECTS

TABLE V
MEAN ERROR COEFFICIENTS OF VARIATION (eCV%) DUE TO CHANGES IN GRID CELL SIZES (5–70 M) FOR ALL LIDAR METRICS CONSIDERED USING THE POINT-CLIP APPROACH

Metric	eCV%	metric	eCV%	metric	eCV%	metric	eCV%	metric	eCV%	metric	eCV%
xyMnRt	0	xySdRt	1.21	htRt_20_30	2.38	surfAreaScl	4.91	anisotropy	13.31	xyCvRt	66.57
xyMinRt	0	xyCvRt	1.21	htP60	2.50	xyzMinRt	4.94	htP10	15.41	linearity	71.50
xyMaxRt	0	htRt_5_10	1.21	p3rd	2.52	htP80	5.43	htMax	15.59	eigen_smallest	77.72
yMin	0.01	htP40	1.26	p4th	2.69	htSdScl	5.55	htIQ	16.75	xyzCor	82.41
yMax	0.01	htCover_1	1.27	htRt20	2.92	xyzMaxRt	6.09	htMeanRt	18.67	htMinRt	84.46
htRt1	0.02	htRt4	1.39	p5th	2.93	htRt_1_2	7.23	htP5	22.53	xyArea	93.85
xyMaxRt	0.04	yRtHt	1.49	htRt_4_5	3.30	htP90	7.29	htMin	24.83	gridVol	96.10
xyMnRt	0.04	xRtHt	1.51	gridVolScl	3.39	htP20	8.04	htP1	30.60	voxVol	96.12
xyMinRt	0.05	htRt5	1.62	htRt_30_50	3.51	htP95	8.73	curvature	32.05	surfArea	97.42
xMax	0.08	p2nd	1.73	xyzSdRt	3.52	voxVolScl	9.03	sphericity	38.84	eigen_medium	100.12
xMin	0.09	htRt_10_20	1.74	htRt30	3.59	xyzCvRt	9.79	horizontality	44.03	xyCor	113.83
areaCover	0.36	xyzCvRt	1.75	htP70	3.98	htCv	9.85	planarity	49.83	xyCorRt	198.99
htRt2	0.74	htCvRt	1.89	htP30	4.02	xyzSdRt	10.95	eigen_largest	63.38	xyzCorRt	310.23
htP50	0.86	htMean	2.19	htRt50	4.30	htP99	11.37	ySd	66.51		
xyzMnRt	0.97	htIQRt	2.24	htRt_50_200	4.30	xyzMnRt	11.92	xSd	66.52		
p1st	1.13	htRt10	2.38	htRt_2_4	4.65	htSd	13.25	xySdRt	66.55		

Large values of eCV% indicate increased sensitivity to size and scale effects.

REFERENCES

[1] J. Vauhkonen, M. Maltamo, R. E. Mcroberts, and E. Næsset, *Forestry Applications of Airborne Laser Scanning*, vol. 27. Berlin, Germany: Springer, 2014, doi: 10.1007/978-94-017-8663-8.

[2] E. Kotivuori, M. Maltamo, L. Korhonen, J. L. Strunk, and P. Packalen, "Prediction error aggregation behaviour for remote sensing augmented forest inventory approaches," *Forestry, Int. J. Forest Res.*, vol. 94, no. 4, pp. 576–587, Aug. 2021, doi: 10.1093/forestry/cpab007.

[3] D. N. Cosenza et al., "Comparison of linear regression, k-nearest neighbour and random forest methods in airborne laser-scanning-based prediction of growing stock," *Forestry, Int. J. Forest Res.*, vol. 94, no. 2, pp. 311–323, Apr. 2021, doi: 10.1093/forestry/cpaa034.

[4] J. L. Strunk and R. J. McGaughey, "Stand validation of lidar forest inventory modeling for a managed southern pine forest," *Can. J. Forest Res.*, vol. 53, no. 2, pp. 71–89, Jan. 2023, doi: 10.1139/cjfr-2022-0032.

[5] V. Kankare, X. Liang, M. Vastaranta, X. Yu, M. Holopainen, and J. Hyyppä, "Diameter distribution estimation with laser scanning based multisource single tree inventory," *ISPRS J. Photogram. Remote Sens.*, vol. 108, pp. 161–171, Oct. 2015, doi: 10.1016/j.isprsjprs.2015.07.007.

[6] S. M. Jeronimo, D. J. Churchill, R. Mcgaughey, and J. F. Franklin, "Applying LiDAR individual tree detection to management of structurally diverse forest landscapes," *J. Forestry*, vol. 116, pp. 336–346, Jun. 2018, doi: 10.1093/jofore/fvy023.

[7] A. M. Sparks and A. M. S. Smith, "Accuracy of a LiDAR-based individual tree detection and attribute measurement algorithm developed to inform forest products supply chain and resource management," *Forests*, vol. 13, no. 1, pp. 1–15, Jan. 2022, doi: 10.3390/f13010003.

[8] M. Vastaranta, V. Kankare, M. Holopainen, X. Yu, J. Hyyppä, and H. Hyyppä, "Combination of individual tree detection and area-based approach in imputation of forest variables using airborne laser data," *ISPRS J. Photogram. Remote Sens.*, vol. 67, pp. 73–79, Jan. 2012, doi: 10.1016/j.isprsjprs.2011.10.006.

[9] P. Packalen, J. Strunk, T. Packalen, M. Maltamo, and L. Mehtätalo, "Resolution dependence in an area-based approach to forest inventory with airborne laser scanning," *Remote Sens. Environ.*, vol. 224, pp. 192–201, Apr. 2019, doi: 10.1016/j.rse.2019.01.022.

[10] C. A. G. Crawford and L. J. Young, "Change of support: An interdisciplinary challenge," in *Geostatistics for Environmental Applications*, P. Renard, H. Demougeot-Renard, and R. Froidevaux, Eds. Berlin, Germany: Springer, 2005, pp. 1–13. doi: 10.1007/3-540-26535-X_1.

[11] N. D. Rayl et al., "Modeling elk-to-livestock transmission risk to predict hotspots of brucellosis spillover," *J. Wildlife Manage.*, vol. 83, no. 4, pp. 817–829, 2019, doi: 10.1002/jwmg.21645.

[12] A. Baddeley et al., "Spatial logistic regression and change-of-support in Poisson point processes," *Electron. J. Statist.*, vol. 4, pp. 1151–1201, Jan. 2010, doi: 10.1214/10-EJS581.

[13] P. C. Kyriakidis and E.-H. Yoo, "Geostatistical prediction and simulation of point values from areal data," *Geographical Anal.*, vol. 37, no. 2, pp. 124–151, 2005.

[14] P. M. Atkinson, "Spatial scale, problems of," in *Encyclopedia of Social Measurement*. Amsterdam, The Netherlands: Elsevier, 2005, pp. 639–648. doi: 10.1016/B0-12-369398-5/00355-8.

[15] E. W. Mauya, E. H. Hansen, T. Gobakken, O. M. Bollandsås, R. E. Malimbwi, and E. Næsset, "Effects of field plot size on prediction accuracy of aboveground biomass in airborne laser scanning-assisted inventories in tropical rain forests of Tanzania," *Carbon Balance Manage.*, vol. 10, pp. 1–14, 2015.

[16] P. Packalen, J. Strunk, M. Maltamo, and M. Myllymäki, "Circular or square plots in ALS-based forest inventories—Does it matter?," *Forestry, Int. J. Forest Res.*, vol. 96, pp. 49–61, Sep. 2022, doi: 10.1093/forestry/cpac032.

[17] F. Mauro et al., "Regional modeling of forest fuels and structural attributes using airborne laser scanning data in Oregon," *Remote Sens.*, vol. 13, no. 2, Jan. 2021, Art. no. 261, doi: 10.3390/rs13020261.

[18] H.-E. Andersen, J. L. Strunk, and R. J. McGaughey, "Using high-performance global navigation satellite system technology to improve forest inventory and analysis plot coordinates in the Pacific Region," Gen. Tech. Rep. PNW-GTR-1000, vol. 1000, 2022.

[19] G. W. Frazer, S. Magnussen, M. A. Wulder, and K. O. Niemann, "Simulated impact of sample plot size and co-registration error on the accuracy and uncertainty of LiDAR-derived estimates of forest stand biomass," *Remote Sens. Environ.*, vol. 115, no. 2, pp. 636–649, Feb. 2011, doi: 10.1016/j.rse.2010.10.008.

[20] A. Pascual, J. Guerra-Hernández, D. N. Cosenza, and V. Sandoval, "The role of improved ground positioning and forest structural complexity when performing forest inventory using airborne laser scanning," *Remote Sens.*, vol. 12, no. 3, pp. 1-22, Jan. 2020, doi: 10.3390/rs12030413.

[21] W. R. Tobler, "Frame independent spatial analysis," in *Accuracy of Spatial Databases*. Boca Raton, FL, USA: CRC Press, 1989, pp. 115–122.

[22] D. E. Jelinski and J. Wu, "The modifiable areal unit problem and implications for landscape ecology," *Landscape Ecol.*, vol. 11, pp. 129–140, 1996.

[23] S.-I. Lee, M. Lee, Y. Chun, and D. A. Griffith, "Uncertainty in the effects of the modifiable areal unit problem under different levels of spatial autocorrelation: A simulation study," *Int. J. Geographical Inf. Sci.*, vol. 33, no. 6, pp. 1135–1154, 2019.

[24] U. Y. Ozkan and T. Demirel, "The influence of window size on remote sensing-based prediction of forest structural variables," *Ecological Processes*, vol. 10, no. 1, pp. 1–11, Sep. 2021, doi: 10.1186/s13717-021-00330-4.

[25] W. A. Bechtold and P. L. Patterson, Eds., *The Enhanced Forest Inventory and Analysis Program: National Sampling Design and Estimation Procedures*. Asheville, NC, USA: US Dept. Agric. Forest Service, Southern Research Station, 2005.

[26] G. E. Dixon, "Essential FVS: A user's guide to the forest vegetation simulator," Forest Management Service Center, Fort Collins, CO, USA, Aug. 2022. Accessed: May 2, 2023. [Online]. Available: https://www.fs.usda.gov/fmsc/ftp/fvs/docs/gtr/EssentialFVS.pdf

[27] J.-R. Roussel et al., "lidR: An R package for analysis of airborne laser scanning (ALS) data," *Remote Sens. Environ.*, vol. 251, Dec. 2020, Art. no. 112061, doi: 10.1016/j.rse.2020.112061.

[28] J. L. Strunk, "RSForTools," Sep. 1, 2024. [Online]. Available: https://github.com/jstrunk001/RSForTools

[29] R Core Team, "R: A language and environment for statistical computing," Vienna, Austria, Manual, 2020. [Online]. Available: https://www.R-project.org/

[30] G. M. Furnival and R. W. Wilson Jr., "Regressions by leaps and bounds," *Technometrics*, vol. 16, no. 4, pp. 499–511, 1974.

[31] T. Lumley, "leaps: Regression subset selection based on Fortran code by Alan Miller," 2017. [Online]. Available: https://CRAN.R-project.org/package=leaps

[32] C.-E. Särndal, B. Swensson, and J. Wretman, *Model Assisted Survey Sampling*. Berlin, Germany: Springer, 2003.

[33] N. Knapp, A. Huth, and R. Fischer, "Tree crowns cause border effects in area-based biomass estimations from remote sensing," *Remote Sens.*, vol. 13, no. 8, Jan. 2021, Art. no. 1592, doi: 10.3390/rs13081592.

[34] J. Mascaro, M. Detto, G. P. Asner, and H. C. Muller-Landau, "Evaluating uncertainty in mapping forest carbon with airborne LiDAR," *Remote Sens. Environ.*, vol. 115, no. 12, pp. 3770–3774, 2011.

[35] M. Rejou-Mechain et al., "Local spatial structure of forest biomass and its consequences for remote sensing of carbon stocks," *Biogeosciences*, vol. 11, no. 23, pp. 6827–6840, 2014.